Study of Poling and Relaxation in Kink and Linear Main-Chain-Functionalized Polymers for Second-Order Nonlinear Optical Applications

Lee-Yin Liu and Hilary S. Lackritz*

School of Chemical Engineering, Purdue University, West Lafayette, Indiana 47907-1283

Michael E. Wright* and Sanjoy Mullick

Department of Chemistry & Biochemistry, Utah State University, Logan, Utah 84322-0300

Received October 20, 1994; Revised Manuscript Received January 6, 1995®

ABSTRACT: The rotational dynamics of nonlinear optical chromophores functionalized to polymer main chains were studied using second harmonic generation. Corona poling was used to orient the chromophores into the bulk noncentrosymmetric structure required to observe second-order nonlinearity. In order to detect different microscopic relaxation mechanisms of the polymers, chromophores were incorporated into the polymer main chain but positioned in two different ways. It was found that for a kink polymer, in which the chromophores were directed at an angle away from the major molecular axis of the polymer chain, the motion of the tilted chromophores may occur through local segmental motion. For a linear polymer, which had the same chromophore, but placed parallel to the chain direction, a large scale main-chain motion was involved in orientation. Therefore, the end-to-end vectors of the polymer chains could be detected. The temperature dependence of the second-order nonlinearity in these polymers showed that there was an optimum temperature at which the main-chain chromophores could be relatively easily oriented during poling. The retarded polymer mobility at lower temperatures and the enhanced rotational Brownian motion at higher temperatures reduced the degree of the chromophore alignment, and therefore a lower second-order signal was observed during poling. Dielectric relaxation spectroscopy showed that the bulk conductivity and crystallinity might also contribute to the decrease in second-order nonlinearity observed at high temperatures.

Introduction

The successful design and synthesis of nonlinear optical (NLO) polymers for practical applications is a growing area of intense research.[1] Many synthetic and processing schemes have been used to optimize nonlinear optical chromophore (NLO-phore) and polymer system construction to maximize the thermal and temporal stability of polymers for second-order nonlinear optical applications.[2] An important study of nonlinear optical polymer systems involves the incorporation of the chromophore as part of the polymer backbone.[3,4] In functionalized systems, it is expected that the thermal or temporal stability of the chromophore orientation following poling would be improved because of decreased mobility of the chromophores in the polymer matrix.[5,6] However, by comparing the rotational dynamics of an identical NLO-phore during and following poling in a main-chain- and side-chain-functionalized polymer and a guest–host system, relaxation studies have shown consistently that the side-chain polymers show the greatest long-term stability.[7,8] The limited second order nonlinearity of a main-chain functionalized polymer may be caused by inadequate polymer structure design, which may result in relatively poor processing properties of the material.

Recent studies at Kodak[6,9] attempted to relate the observed thermal dependence of the second harmonic generation (SHG) intensity to polymer mobility and relaxations measured using thermally stimulated current techniques and dielectric relaxation for side-chain- and main-chain-functionalized polymers. They found that the reorientation of the polar chromophores functionalized to the side chain occurred through local polymer relaxation, but if the chromophores were functionalized into the backbone, then the reorientation of the end-to-end vectors of the chains was involved. Katz and co-workers[10] have detected an increase in the net dipole moment upon linking dipolar units together in the main-chain-functionalized polymers. Dalton and co-workers[11] have also shown that alignment of the main-chain-functionalized chromophores was possible by random orientation of main-chain polyurethane during corona poling. Francis and co-workers[12] have also detected SHG activity in head-to-tail dipolar NLO polymers.

In order to have a better understanding of the microscopic relaxation mechanisms that affect the rotational dynamics in main-chain functionalized polymers, two novel polymers were synthesized using the Knoevenagel polycondensation. An identical NLO-phore was incorporated into the polymer main chain but positioned in different ways in different polymers. In one of the polymers, the orientation of the dipolar units is tilted an angle away from the major direction of the chain axis, resulting in a "kink" along the polymer chain. The other polymer has its dipoles parallel to the chain axis and therefore has a linear configuration. Since the NLO-phores are restricted by polymer configuration, different types of motion in a polymer system can be understood by examining the motion of the NLO-phores.

The rotational dynamics of the NLO-phores was monitored using second harmonic generation.[13] Corona poling was used to orient the NLO-phores into the bulk noncentrosymmetric structure required to observe second-order nonlinearity. The magnitude of $\chi^{(2)}$, the second-order susceptibility, was calculated from the second harmonic signal. Since the magnitude of $\chi^{(2)}$ is related

* To whom correspondence should be addressed.

® Abstract published in *Advance ACS Abstracts,* February 15, 1995.

0024-9297/95/2228-1912$09.00/0

Scheme 1

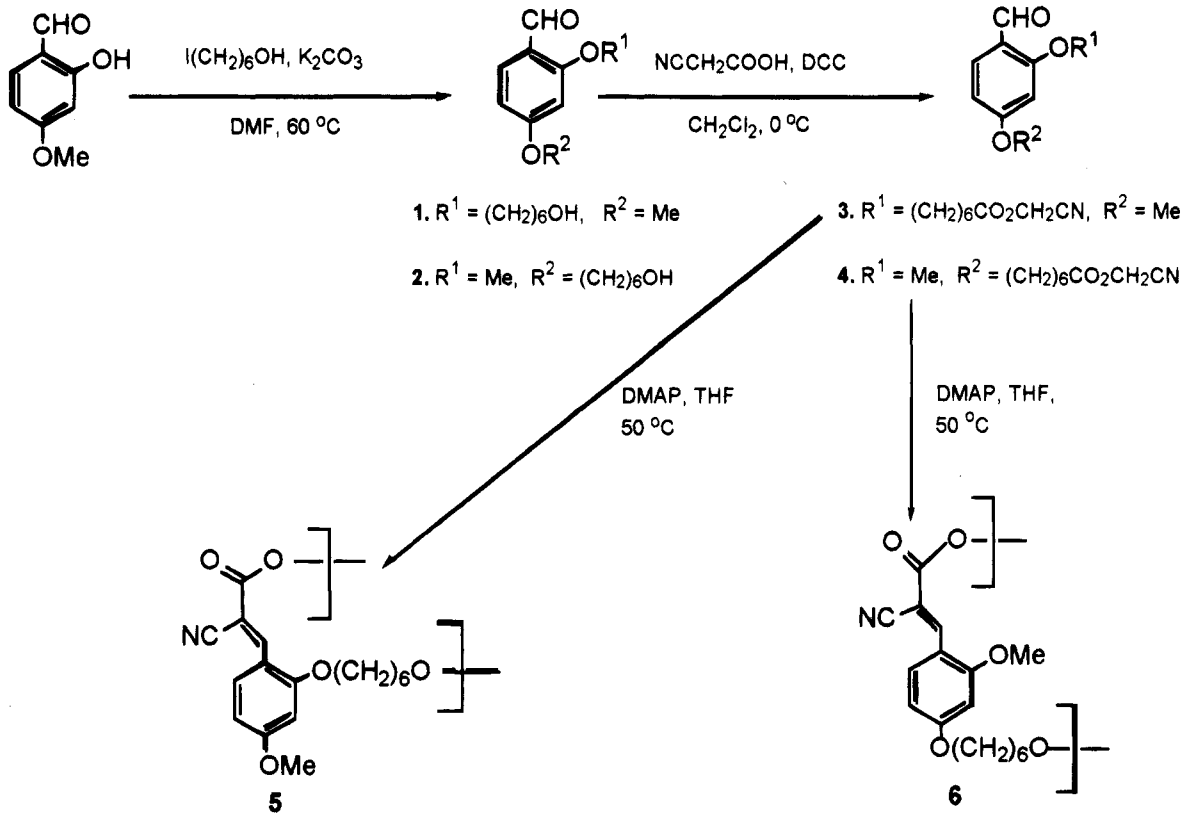

to the degree of the alignment of NLO-phores,[14] different relaxation mechanisms in a polymer that govern the mobility of the NLO-phores could be investigated by examining $\chi^{(2)}$ over a wide range of temperature and time.

In this study, dielectric relaxation spectroscopy was also used to examine the dipole-associated polymer relaxations in these polymers. Dielectric relaxation measurements are useful because they work well in highly packed dipolar materials, give information about the conductivity, and directly measure the ground-state dipole motion.[9] A comparison between second harmonic generation and dielectric relaxation will give a more complete analysis concerning local mobility and relaxation mechanisms in these polymers.

Results and Discussion

Monomer Synthesis. Treatment of 2-hydroxy-4-methoxybenzaldehyde with 6-iodohexanol in the presence of potassium carbonate afforded compound **1** in good yields (Scheme 1). Compound **1** was then reacted with cyanoacetic acid and dicyclohexylcarbodiimide (DCC) to afford monomer **3** in quantitative yields.[15] Flash chromatography on deactivated alumina was avoided because this led to polymerization of the monomer on the column. Purification was performed by oiling the material out of ethyl acetate with hexanes (1/2, v/v).

Monomer **4** was prepared in a similar straightforward manner, starting with 4-hydroxy-2-methoxybenzaldehyde in quantitative yields (Scheme 1) and also purified in a similar manner to that of monomer **3**. The monomers are stable only when stored at −25 °C. If kept at ambient temperature, the monomers are unstable and have a tendency to homopolymerize even under neutral conditions.

Polymer Synthesis and Characterization. Monomers **3** and **4** were homopolymerized using the Knoevenagel polycondensation technique (Scheme 1).[7] For the kink polymer **5**, a bimodal molecular weight distribution was obtained which was initially in the ratio of 1:1 of the high to the low molecular weight. Separation of the high molecular weight fraction from the low molecular weight species was attempted. The best enrichment was obtained with acetonitrile as the solvent and with selective precipitation of the higher molecular weight species representing around 89% of the material (based on UV−vis absorption data in the GPC trace). For the linear polymer **6**, a unimodal molecular weight distribution was observed. The polymers are readily soluble in a variety of solvents; CH_2Cl_2, $CHCl_3$, benzene, diethyl ether (~10% by weight). A typical polymerization run would produce the following data (Table 1): for the enriched polymer **5** M_n = 14 700, D_p = 49, PD = 1.8 and M_n = 1600, PD = 1.4; for **6** M_n = 19 000, D_p = 63, PD = 1.4. Polymers are light yellow in color with λ_{max} absorption at 370 nm. The geometry about the double bond has been found to be consistent with the (*E*)-olefin upon inspection of the NMR spectral data of the polymers.

Table 1. Selected Physical and Spectroscopic Data for Polymers 5 and 6

polymer	M_n	M_w	UV−vis (CH_2Cl_2)	TGA (°C) (break point)[a]
5	14 700	27 000	λ_{max} = 370 nm ($\epsilon = 14.5 \times 10^3$)	332
6	19 000	26 000	λ_{max} = 370 nm ($\epsilon = 18.8 \times 10^3$)	318

[a] Under a nitrogen atmosphere, ramp rate of 10 °C/min. The break point is the temperature where a continuous and rapid weight loss begins to occur.

Both polymers **5** and **6** are regioisomers, differing in the position of the polymerizable groups. The difference in the molecular weight distribution between the two polymers can be explained in terms of cyclization of the growing polymer chain that terminates the polymeri-

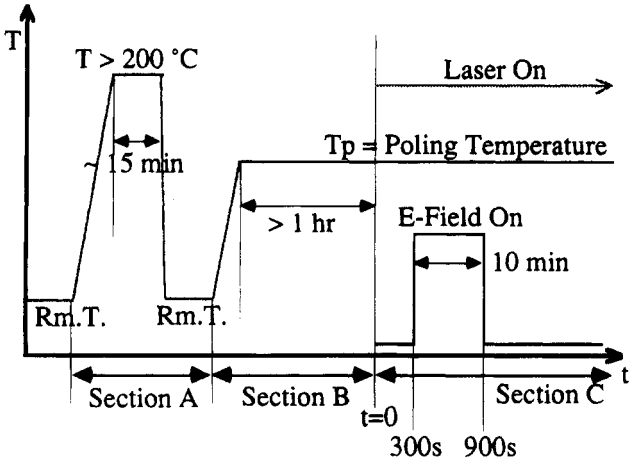

Figure 1. Thermal treatment of the polymers and SHG measurement procedure.

zation process. The hybridization at the double bond in the aldehydic carbon changes from a sp^2 to a sp^3 carbon leading to an increase in the bond angle as the condensation proceeds. Consequently, this increase in the bond angle also leads to an increase in the mobility of the flexible polymer chains which can now easily cyclize at the adjacent carbon atom, thereby forming low molecular weight oligomers. On the other hand, a certain proportion of the growing polymer chains may not cyclize, and hence high molecular weight polymers are formed. This bimodal distribution of the molecular weights was also observed in our previous work.[7] In the case of the linear polymer cyclization is not possible in the growing polymer chain and hence only a unimodal distribution of molecular weight is observed.

Thermal analysis of the polymer was carried out under a nitrogen atmosphere. Differential scanning calorimetry (DSC) revealed an initial T_g or a T_m due to the purification process from the first scans. The scanning rate was 10 °C/min, and the results were obtained from heating scans. Subsequent DSC scans by heating and rapid cooling of the polymers (at the rate of −20 °C/min) erased the melting points of the samples, indicating a loss of crystallinity. This was also true in the case of slow cooling (at −5 °C/min). This indicates that it is possible to quench the polymers to a glassy state by rapid or even slow cooling.

Thermal gravimetric analysis (TGA) of the polymer was performed. Both the polymers are stable at 260+ °C. The break points of the polymer thermal decomposition occur at 332 and 318 °C for **5** and **6**, respectively (Table 1).

SHG Evaluation of the Polymers. Three kink (polymers **5−1**, **5−2**, and **5−3**) and one linear (polymer **6**) main-chain-functionalized polymers of identical NLO-phore but with different molecular weight ratios were synthesized for second harmonic generation measurements. The linear polymer has a unimodal molecular weight distribution. Polymers **5−1** and **5−3** are the enriched polymers of polymer **5** with the high to low molecular weight ratio of 7:1 and 2:1, respectively. Polymer **5−2** is the unfractionated polymer **5** with the molecular weight ratio of 1.4:1. In the following sections, polymer **5−1** is also specified as the high, polymer **5−2** as the low, and polymer **5−3** as the medium molecular weight kink polymer.

In the linear polymer, the NLO-phore is incorporated into the polymer main chain with the dipole moment of the NLO-phore placed parallel to the molecular axis of the polymer backbone (Scheme 1). The kink polymer has the same NLO-phore on the main chain as that in the linear one but has the NLO-phore dipole tilted an angle away from the direction of the molecular axis of the polymer chain (Scheme 1). Because both kinds of polymers have the same NLO-phores with similar loadings, optical and physical effects that vary from chromophore to chromophore are eliminated, and the polymer mobility is the dominant feature considered when comparing experimental trends. It is expected that the motion of the NLO-phores in the linear polymer is more related to the global motion of the polymer chain than that in the kink system, in which the motion of the tilted NLO-phores may occur through local segmental motion.[6] By examining the second harmonic signal as a function of temperature and time in these polymers, the effects of different types of motion of the polymer chain on the NLO-phore mobility can be investigated.

Table 2. Maximum $\chi^{(2)}$ Obtained during Corona Poling for the Main-Chain-Functionalized Polymers

	kink			linear
T_p[a] (°C)	polymer **5−1**	polymer **5−2**	polymer **5−3**	polymer **6**
64	0.095[b,c]	0.136	0.120	0.170
137	0.09	0.10	0.10	0.124

[a] Poling temperature. [b] The maximum $\chi^{(2)}$ value (in units of pm/V) obtained during corona poling. [c] Accuracy: ±12%.

Polymer solutions (5 wt %) were prepared and spin-cast onto indium−tin−oxide (ITO)-coated glass slides to form uniform thin films. The films were dried carefully under identical conditions to remove as much solvent as possible.[13] Isothermal second-order nonlinear optical properties were measured using second harmonic generation with a 1064 nm fundamental frequency. The UV−vis spectroscopy showed that no absorption was observed at the harmonic frequency for the dried polymer films. The experimental apparatus was described elsewhere.[7] The films were subjected to corona poling[7,16] (+4 kV, 1 cm air gap) for 10 min.

In order to orient the NLO-phores during poling in these main-chain-functionalized polymers, a preheating and quenching thermal treatment (Figure 1, section A) is required to remove any residual crystallinity and to achieve the glassy state in the systems. DSC data (10 °C/min) show no apparent T_g or T_m's for the preheated and quenched polymers. The thermally treated polymer films give a significant $\chi^{(2)}$ response upon the application of the external dc poling field. However, no significant $\chi^{(2)}$ signal is detected for the polymers before the thermal treatment. We believe that before thermal treatment small amounts of crystallinity exist in the material (first DSC scan shows small T_m peak). The NLO-phores cannot be oriented in a crystalline matrix.

The maximum $\chi^{(2)}$ values obtained during poling are listed in Table 2. Table 2 shows that for the kink systems the low molecular weight polymer **5−2** gives relatively the largest second-order NLO response to the poling field within the experimental error. This is because the low molecular weight polymer, in which more flexible chain ends are present, has the highest local mobility per unit volume. The motion of the internal chain segments is more correlated and therefore more restricted or hindered. Greater rotational motion of NLO-phores can occur in the areas of greatest local mobility. The higher mobility in the low molecular weight polymer is also observed when comparing the $\chi^{(2)}$ decay rate following corona poling with that of the higher molecular weight polymers. In Figure 2 the $\chi^{(2)}$ relaxation data are normalized to the point when the

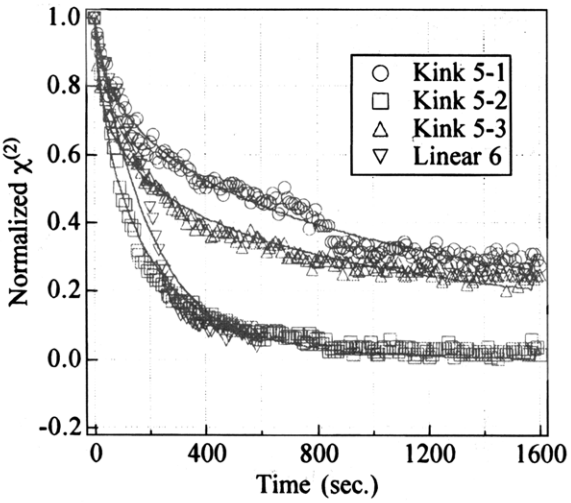

Figure 2. Comparison of the $\chi^{(2)}$ decay following corona poling ($t > 0$) for the main-chain-functionalized polymers at low temperature ($T_p = 64$ °C).

corona voltage is turned off so that the comparison of the decay rates of different polymers can be made. As expected, the high molecular weight polymer **5−1**, which has the least local mobility in the bulk, exhibits the slowest NLO-phore reorientation. This implies that in order to obtain high $\chi^{(2)}$ magnitude during poling and high $\chi^{(2)}$ stability following poling, optimized material design and thermal processing is required. The medium molecular weight polymer **5−3** gives about the same $\chi^{(2)}$ magnitude as the low molecular weight polymer but shows an enhanced $\chi^{(2)}$ stability similar to that of the high molecular weight one (Figure 2).

In Table 2 it is observed that the linear polymer gives the greatest $\chi^{(2)}$ magnitude during poling as compared to those of the kink systems. It is believed that a large scale or global main-chain motion may occur in the linear polymer at or near the poling temperature T_p = 64 °C, at which only local segmental motion is significant in the kink polymers. A large scale main-chain motion could assist the additivity of the dipoles during poling and therefore result in a relatively greater $\chi^{(2)}$ signal.[6] In order to evaluate the likelihood of this possibility, the following argument is considered. The DSC data show that the linear polymer has the lowest T_m (about 60 °C) as compared to that of the kink polymers ($T_m \sim 150-200$ °C) if the polymers are freshly made without any thermal treatment. Although subsequent DSC scans (10 °C/min) reveal the absence of T_g or T_m's in the preheated and quenched polymers, it is reasonable to assume that the linear polymer still has relatively less molecular interaction between polymer chains. Therefore, the polymer chains of the linear polymer are more mobile than those of the kink ones at the poling temperature (64 °C) which is above the T_m of the fresh linear polymer but far below the T_m's of the kink systems. The NLO-phores of the linear polymer can then be oriented through a large scale main-chain motion to give a larger $\chi^{(2)}$ signal than those of the kink ones, in which only local segmental motion is allowed to occur at low temperature. It should be noted that although less $\chi^{(2)}$ signal is observed during poling, the temporal stability of $\chi^{(2)}$ in the kink polymer, especially polymers **5−1** and **5−3**, is greater than that of the linear polymer following poling (Figure 2). Since most of the polymer chain in the kink system is relatively less mobile at T = 64 °C, the rotational motion of the NLO-phores in the kink system is more restricted than that in the linear polymer. This indicates that the presence of a rigid, less mobile moiety in the polymer system is required to retard the NLO-phore reorientation and therefore to enhance the $\chi^{(2)}$ stability following poling.

Table 3. Kohlrausch−Williams−Watts Parameters (τ and β) and the Average Relaxation Times ($\langle\tau\rangle$) of the $\chi^{(2)}$ Decay Following Poling (T_p = 64 °C)

	kink			linear
	polymer **5−1**	polymer **5−2**	polymer **5−3**	polymer **6**
τ (s)	916	152	537	203
β	0.53	0.96	0.42	~1
$\langle\tau\rangle$ (s)	1636	155	1541	203

At the higher poling temperature, T_p = 137 °C, it is found that the linear polymer still gives the greatest $\chi^{(2)}$ signal (Table 2). This may be because the poling temperature is not high enough for the global main-chain motion to occur in the kink systems. However, all the polymers show a lower magnitude of $\chi^{(2)}$ when poled at 137 °C as compared to the low-temperature data (T_p = 64 °C). No significant signal was observed for samples poled at $T > 137$ °C. Competitive rotational Brownian motion of the NLO-phores[17] and enhanced charge injection during corona poling[18] may cause the decrease of poling efficiency at high temperatures. In order to have effective poling, three major factors that affect the orientation distribution of the NLO-phores must be considered: the mobility of the polymer chains, the rotational Brownian motion of the NLO-phores, and the electric field effects. The temperature must be high enough so that there is sufficient local mobility in the polymer system to allow the NLO-phores to have enough freedom to orient in response to the applied field. However, as the temperature increases, the thermal randomizing effect of the rotational Brownian dynamics competes with the orienting effect of the poling field and thus reduces the poling efficiency ($\chi^{(2)} \propto \mu E_p/kT_p$).[14] At the same time, the charges dispersed on the polymer surface during corona poling are more likely to penetrate into the polymer film at high temperature.[18] Bulk conductivity, which can be caused by minute amounts of impurities and other factors, will increase as the temperature increases. This diminishes the net electric field gradient across the polymer film, resulting in the NLO-phores disorienting to a certain extent even with the field still applied. For the temperature range used in this work (64 °C < T < 137 °C), the thermal randomizing effect may only reduce the high-temperature poling efficiency to 80% of that at low temperature. Therefore, the enhanced charge injection and the bulk conductivity may contribute more to the decrease of the magnitude of $\chi^{(2)}$ poled at high temperatures.

The fitting curves of the $\chi^{(2)}$ decay following poling (T = 64 °C) by using the Kohlrausch−Williams−Watts (KWW) equation are shown in Figure 2. The KWW parameters and the average relaxation time for each polymer are listed in Table 3. The KWW equation is frequently used to describe the relaxation behavior in polymers:[19]

$$\varphi(t) = \exp[-(t/\tau)^{\beta}] \quad (1)$$

where $\varphi(t)$ is the relaxation function of interest and τ is the characteristic relaxation time. The index β is related to the broadness of the distribution of relaxation times ($0 \le \beta \le 1$) and $\beta = 1$ corresponds to a single-exponential relaxation. In this case, $\varphi(t)$ is used to fit the time dependence of $\chi^{(2)}$. The average relaxation time

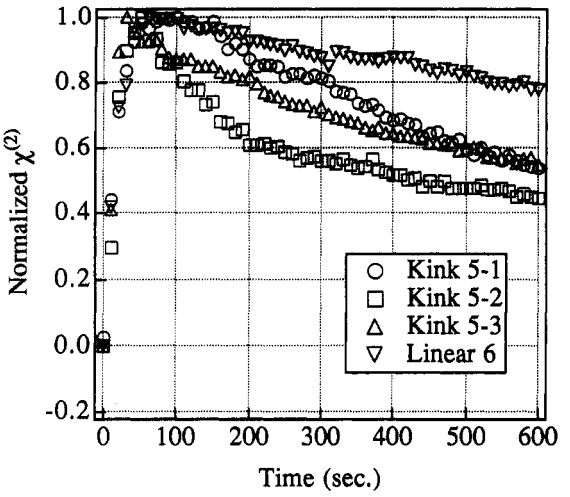

Figure 3. Comparison of the $\chi^{(2)}$ signal during corona poling ($0 < t < 600$ s) for the main-chain-functionalized polymers at high poling temperature ($T_p = 137$ °C).

is defined as[20]

$$\langle\tau\rangle = \tau\Gamma(1/\beta)/\beta \qquad (2)$$

where Γ is the gamma function. It can be seen that the high molecular weight kink polymer **5**−**1** has the longest relaxation time and the low molecular weight kink polymer **5**−**2** has the shortest relaxation time, as expected. The more retarded internal chain segmental motion in the high molecular weight polymer reduces the reorientation rate of the NLO-phores, and therefore a relatively longer corresponding relaxation time is observed. That the linear polymer has a β value close to unity indicates a narrow distribution of relaxation times in this system. This could be related to the unimodal molecular weight distribution in the linear polymer as well as the relatively high relaxation temperature at which the global main-chain motion may occur, resulting in a nearly single-exponential decay. For the kink systems which are relaxed at a relatively low temperature, a smaller β value was observed. This implies a broader distribution of relaxation times, and more different types of molecular motion are involved in the kink polymers. The reorientation of the NLO-phores in the kink systems may occur through the relatively more mobile local motion of the polymer chain segments. For the low molecular weight polymer **5**−**2**, the large β value may result from the presence of more flexible chain ends, which create more local mobility in the system. The restriction of the less mobile internal chain segments on the NLO-phore reorientation becomes more significant in the high molecular weight polymer and therefore results in the broadening of relaxation times and a smaller β value.

Figure 3 shows that the $\chi^{(2)}$ signal decreases during corona poling at high temperatures. This might be caused by thermally excited charge injection, bulk conductivity, or even crystallization in these materials. However, there is no direct evidence from the SHG data that could determine which one is the dominating factor. In Figure 4, the maximum $\chi^{(2)}$ signal obtained during corona poling is plotted versus the poling temperature for the linear polymer **6** and the kink polymer **5**−**2**. It shows that as the poling temperature increases, the $\chi^{(2)}$ magnitude reaches a maximum and then decreases. This is consistent with the argument stated above: an efficient poling process requires an optimum condition in which the three factors (polymer mobility, rotational Brownian motion, and electric field effects) are optimized. Figure 5a,b shows the UV−vis absorption spectrum of the polymer before (fresh) and following (poled) corona poling. The absorption of both the fresh and poled polymer films ranges from about 280 to 430 nm, centering around 350 nm. However, the absorption intensity is decreased throughout the entire range for the poled samples. Extrinsic charge penetration during corona poling may result in this observed phenomenon.[18] The UV−vis data are consistent with the SHG result that the $\chi^{(2)}$ magnitude decreases during corona

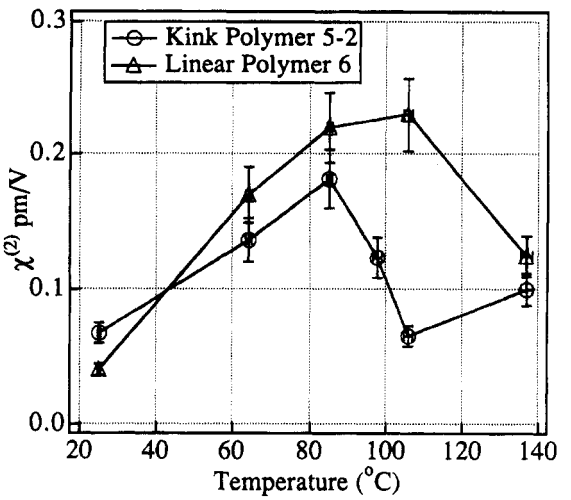

Figure 4. Temperature dependence of the $\chi^{(2)}$ magnitude for the kink and linear polymers.

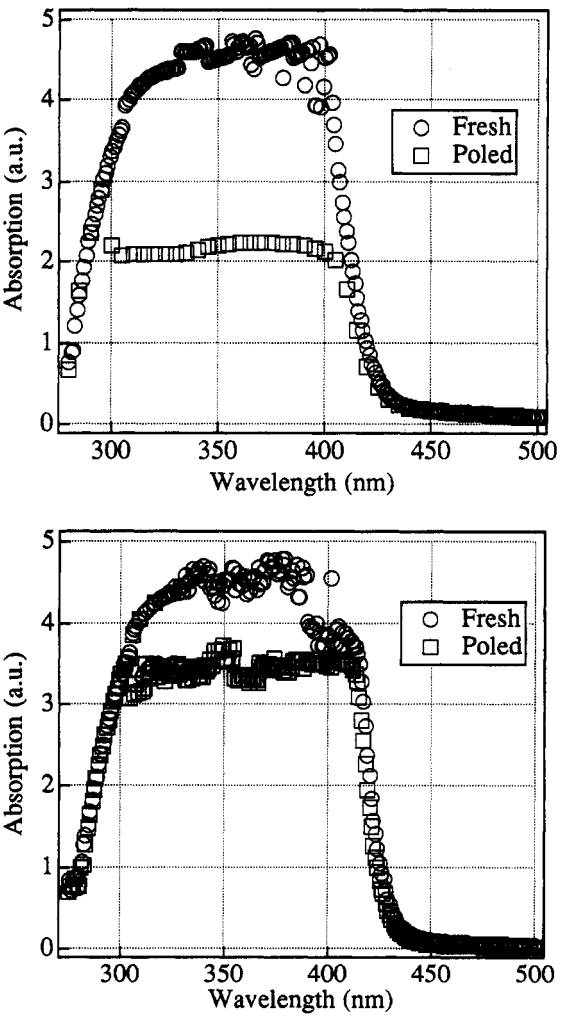

Figure 5. UV−vis spectrum of (a, top) the kink polymer **5**−**3** and (b, bottom) the linear polymer **6** before (fresh) or after (poled) corona poling.

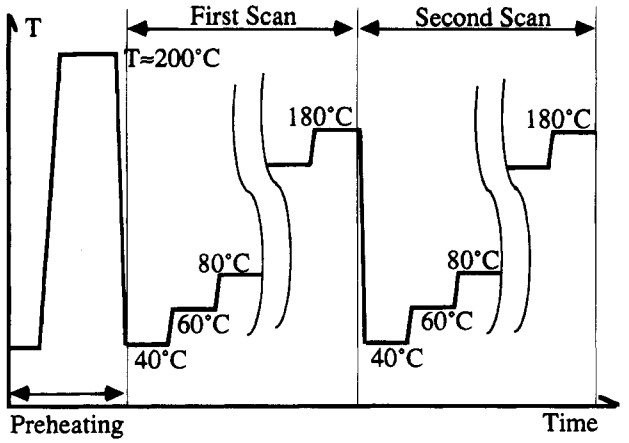

Figure 6. Thermal treatment of the polymers and the dielectric relaxation measurement procedure.

poling for these main-chain-functionalized polymers. The poling efficiency in orienting the NLO-phores is reduced because of charge injection.

Dielectric Relaxation Spectroscopy. In order to obtain a better understanding of main-chain-associated NLO-phore rotational dynamics, dielectric relaxation measurements were also conducted. Dielectric relaxation is an important technique that is frequently used in the study of polymer dynamics.[21] It is useful because it directly measures the motion of the ground-state dipole moments in materials, especially in those possessing high dipole density. It also gives information about the effects of dc and ac conductivity on the response of the dipole moments to the externally applied oscillating electric field. In the main-chain-functionalized nonlinear optical polymers, the dipole moments of the NLO-phores are associated with the polymer main chain. Therefore, by varying the frequency of the applied field, different types of motion with different characteristic relaxation times in the polymer system can then be monitored. Since both the dielectric relaxation and second harmonic generation are related to the rotational motion of the dipoles, a comparison between dielectric and SHG data is helpful for establishing a more complete understanding of the dynamic behavior.

Dry polymer films were prepared in between two ITO-coated glass slides. The ITO slides were used as the electrodes, at which the oscillating electric field was applied. The procedure for dielectric relaxation measurements is schematized in Figure 6. The sample was preheated to remove any residual crystallinity in the polymer. The temperature was increased stepwise during each scan. The isothermal dielectric data were taken as a function of the electric field frequency (f) in each step.

Figure 7 shows the frequency dependence of the real part of the complex dielectric constant (ϵ') for the kink main-chain functionalized polymer **5**–**2**. It is found that the dispersion of ϵ' becomes more significant at higher temperature. At high temperature, the polymer chain is relatively more mobile. Therefore, the dipolar units on the polymer chain can respond to the applied electric field faster (during the low-frequency region) than those at low temperatures. As the frequency increases, the polymer chain cannot respond and retards the orientation of its dipoles. The magnitude of ϵ' thus decreases to the unrelaxed value for all the temperatures.[21] The larger magnitude of ϵ' at low frequencies could result from the high dipole density in this main-chain-functionalized polymer.

The dielectric loss tangent (tan δ) of the polymer is plotted against the field frequency in Figure 8. A

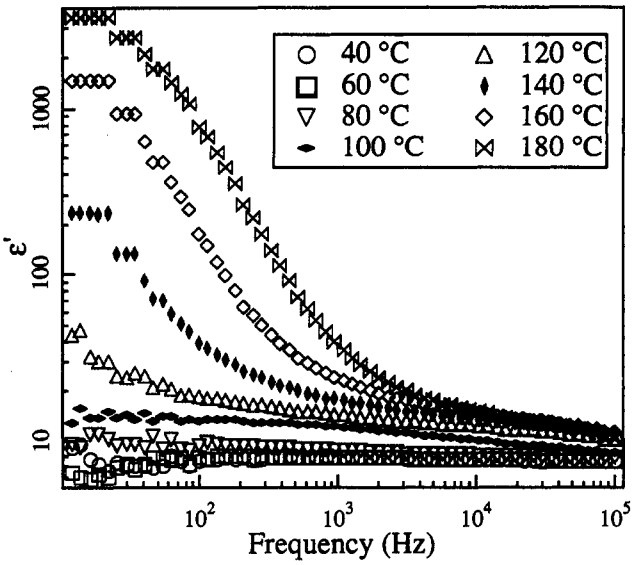

Figure 7. Dielectric constant (ϵ') dispersion in the kink polymer **5**–**2**.

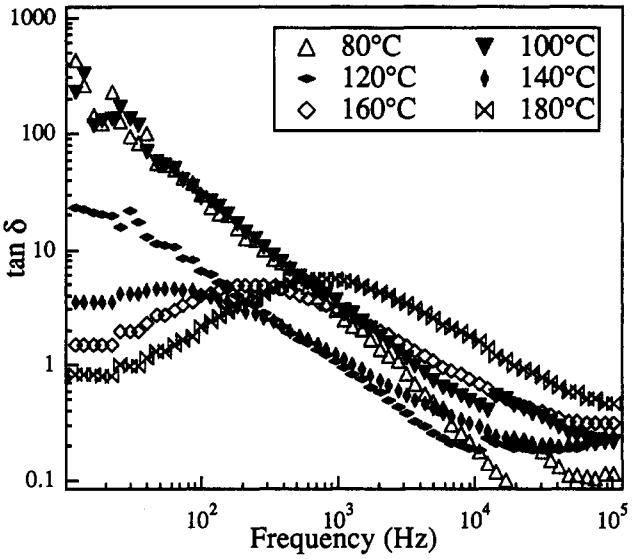

Figure 8. Frequency dependence of the dielectric loss tangent (tan δ) in the kink polymer **5**–**2**.

transition peak is observed at high temperatures (140–180 °C) for the kink polymer. A similar peak is also observed for the linear system, but the peak occurs at lower temperatures (50–80 °C). This peak could be associated with the α glass transition. Since the molecular interaction in the linear system is relatively weak compared with that in the kink polymer, a global main-chain motion may occur and therefore a transition peak is observed at lower temperatures. This observation is consistent with the SHG result. The linear polymer gives a greater $\chi^{(2)}$ signal than the kink polymer during poling. The NLO-phores in the linear polymer could be relatively easily oriented during poling and disorient fast following poling because of its weaker molecular interaction.

Figure 9 shows the dielectric loss factor (ϵ'') of the kink polymer **5**–**2** versus the electric field frequency. It is found that the low-frequency dependence of ϵ'' can be fitted by a straight line with a slope of about −1 in the log–log plot. This dependence in the low-frequency region is primarily caused by the constant dc conductivity (σ_{dc}).[9,21,22] In this dc conductivity regime, ϵ'' is approximately equal to $\sigma_{dc}/2\pi\epsilon_0 f$ (ϵ_0 is the permittivity of free space), and therefore a linear dependence of ϵ''

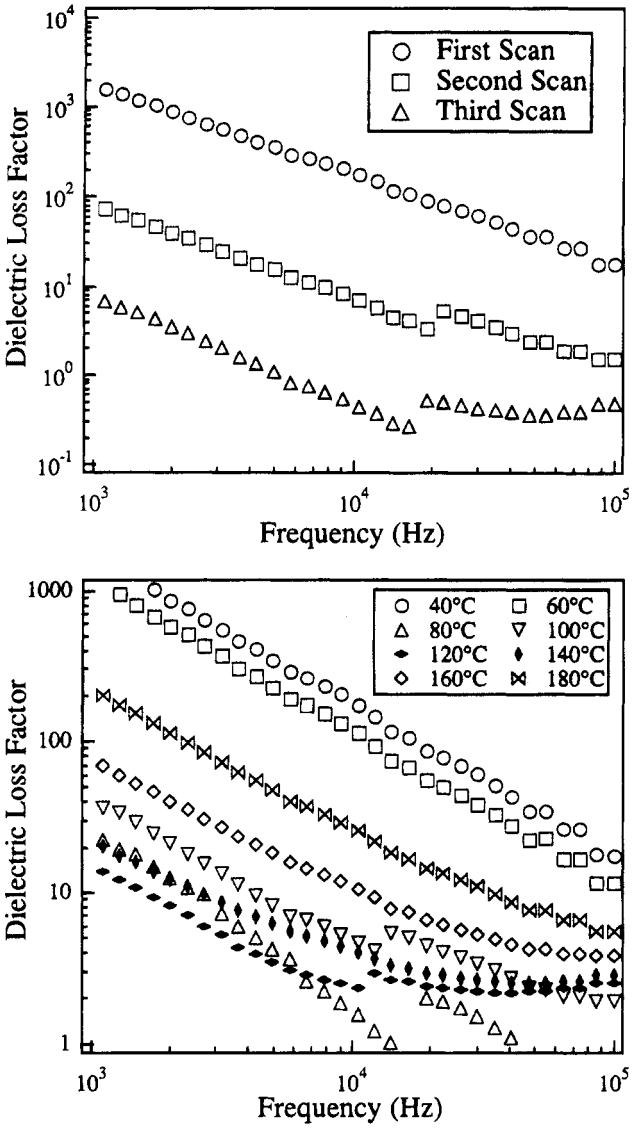

Figure 9. Frequency dependence of the dielectric loss factor ϵ'' in the kink polymer **5** at different temperatures.

on low frequency with a slope of −1 is observed on the log−log scale. The magnitude of the dc conductivity is related to the poling efficiency. It becomes harder to orient the NLO-phores as the conductivity increases ($\chi^{(2)} \propto \mu E_p/kT_p$).

The calculated dc conductivity of the kink polymer **5**−**2** and the linear polymer **6** is plotted versus $1/T$ in Figure 10. It is found that at high temperatures (120−180 °C), the temperature dependence of the dc conductivity can be fitted by the Arrhenius equation.[9,22] However, the dc conductivity deviates from the Arrhenius fit and the temperature dependence becomes irregular at low temperatures. For the kink polymer, an increase in the conductivity occurs near 100 °C when the temperature is either cooled from 120 °C or heated from 80 °C. As compared to the $\chi^{(2)}$ data in Figure 4, the decreased magnitude of $\chi^{(2)}$ near 100 °C may correspond to the increased conductivity near the same temperature. For the linear polymer, the enhanced conductivity above 100 °C may also contribute to the decrease in the magnitude of $\chi^{(2)}$ at high temperatures. The increased conductivity in the material assists the charge penetration during corona poling and therefore reduces the net electric field gradient across the polymer film. The efficiency of poling in orienting the NLO-phores is decreased when the conductivity is high and thus less second harmonic signal is observed.

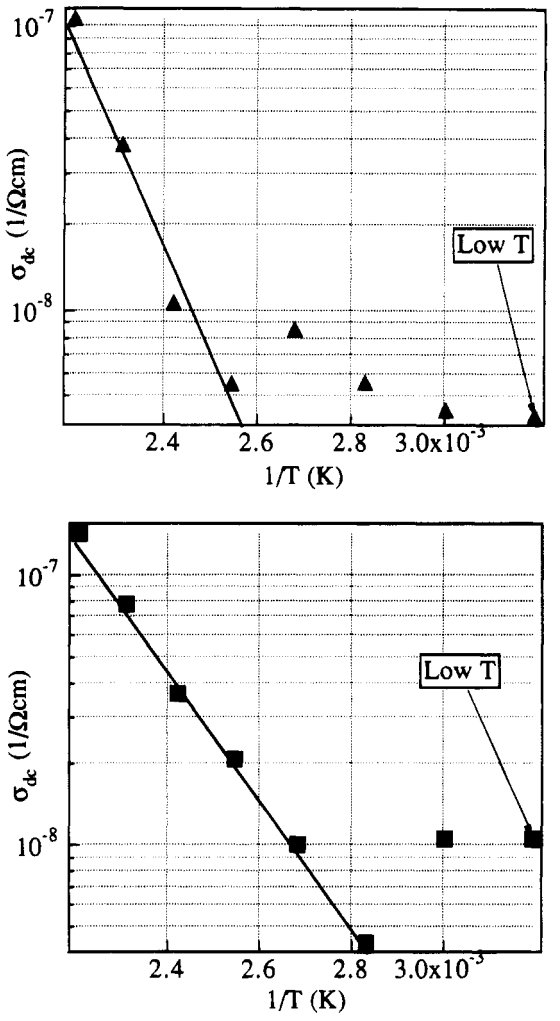

Figure 10. Temperature dependence of the dc conductivity for (a, top) the kink polymer **5**−**2** and (b, bottom) the linear polymer **6**. The straight line is the Arrhenius fit.

The comparison of dielectric relaxation and second harmonic generation shows a consistent result. Both techniques are sensitive in probing the dipole-associated motion in polymers. The greater $\chi^{(2)}$ signal during poling and the faster $\chi^{(2)}$ decay following poling for the linear polymer may result from the weaker molecular interaction in the linear system. This possibility is also observed in the dielectric loss tangent spectrum in which a glass transition peak occurs at lower temperatures for the linear polymer. The high conductivity measured at high temperatures, by using dielectric relaxation indicates the reduction of the poling efficiency in orienting the NLO-phores. Combination of these two methods would give a more detailed investigation of the rotational dynamics in polymers for second-order optical applications.

Conclusions

In this work we have prepared two novel main-chain-functionalized polymers with the same NLO-phore but directed differently in the polymer chain. Second harmonic generation measurements were performed to compare the rotational dynamics of the NLO-phores in these polymers. By use of a preheating and quenching thermal treatment to remove any residual crystallinity in the material, the main-chain NLO-phores had more local mobility to be oriented by the poling field and therefore a significant $\chi^{(2)}$ signal was observed.

It was found that for the linear polymer, in which the main-chain NLO-phores were placed parallel to the

major molecular axis of the polymer chain, the orientation of the NLO-phores could involve a global main-chain motion because of the relatively weak molecular interaction between the polymer chains. The net dipole moment along the polymer chain could be increased through a large scale chain motion in the linear polymer. A greater $\chi^{(2)}$ signal during poling was observed in the linear polymer as compared to that of the kink system. In the kink polymer, the orientation of the dipolar units deviates from the chain axis. Therefore, the rotational motion of the NLO-phores could occur through a local segmental motion at a relatively low temperature. The reorientation of the NLO-phores following poling in the kink polymer, especially the high molecular weight one, was slower than that in the linear polymer. This could result from the stronger molecular interaction of the kink system. This observation provides valuable insights for future polymer synthesis and processing optimization. By modifying the ratio of the flexible and the rigid portion in a polymer, the magnitude and the stability of the $\chi^{(2)}$ signal could be controlled to satisfy any particular application.

The dc conductivity in these polymers was examined by using dielectric relaxation measurements. It was found that enhanced conductivity and crystallization may also contribute to the reduction of the poling efficiency at high temperatures. The temperature dependence of the conductivity in these polymers can be fitted by the Arrhenius law in the high-temperature region. At low temperatures, the magnitude of the conductivity deviated from the Arrhenius line and became irregularly distributed on a log–log plot. However, this distribution was found to be consistent with the temperature dependence of the $\chi^{(2)}$ magnitude in these main-chain-functionalized polymers. Conductivity reduces the field gradient in the material and therefore decreases the poling efficiency in orienting the NLO-phores.

Experimental Section

Methods. All manipulations of compounds and solvents were carried out using the standard Schlenk techniques. Solvents were degassed and purified by distillation under nitrogen from standard drying agents. Spectroscopic measurements utilized the following instrumentation: ^{1}H NMR, Varian XL 300; ^{13}C NMR, JOEL-270, Varian XL 300 (at 75.4 MHz); infrared, Perkin-Elmer 1750 FT-IR; UV–vis, HP-8452A. NMR chemical shifts are reported in δ versus Me_4Si in ^{1}H NMR, and the $CDCl_3$ resonance is assigned at 77.00 ppm in ^{13}C spectra. Dicyclohexylcarbodiimide (DCC), 4-(dimethylamino)pyridine (DMAP), 6-chlorohexanol, cyanoacetic acid, and 2-hydroxy-4-methoxybenzaldehyde were purchased from Aldrich Chemical Co. 4-Hydroxy-2-methoxybenzaldehyde was purchased from Lancaster Synthesis, and all were used as received. K_2CO_3 (granular, AR grade, Mallinckrodt) was purchased from Baxter. Thermal analysis of the polymer was performed using a Perkin-Elmer TGA7 and DSC7 station. GPC data were collected on a HPLC unit consisting of a Beckman pump, Perkin-Elmer detector, and a Hewlett Packard plotter and employing a PL size-exclusion column (300 × 7.5 mm, 5 μm particle size.). Molecular weight data are referenced relative to polystyrene standards. Elemental analyses were performed at Atlantic Microlab Inc., Norcross, GA.

Preparation of 1. A DMF (20 mL) solution of 2-hydroxy-4-methoxybenzaldehyde (2.50 g, 16.4 mmol) was treated with 6-iodohexanol (3.70 g, 16.4 mmol) and K_2CO_3 (7.00 g, 50.0 mmol). The reaction mixture was allowed to react at 60 °C with stirring for 12 h. The mixture was diluted with water (100 mL) and extracted with ether (2 × 150 mL). The organic layers were combined, washed with brine, and dried over anhydrous $MgSO_4$. The solvents were removed under reduced pressure, and the crude product was recrystallized from EtOAc/hexanes (1/5, v/v) to afford an off-white microcrystalline solid (3.07 g, 74%, mp 58–59 °C). ^{1}H NMR ($CDCl_3$): δ 10.33 (s, 1 H, CHO), 7.82 (d, J = 8.7 Hz, 1 H, Ar), 6.54 (dd, J = 2.2 Hz, J = 8.7 Hz, 1 H, Ar), 6.44 (d, J = 2.2 Hz, 1 H, Ar), 4.05 (t, J = 6.3 Hz, 2 H, CH_2OAr), 3.88 (s, 3 H, CH_3), 3.69–3.67 (m, 2 H, CH_2OH), 1.90–1.47 (m, 8 H, CH_2's). ^{13}C NMR ($CDCl_3$): δ 188.5 (CHO), 166.1, 163.2 (Ar C), 130.2 (Ar CH), 118.8 (Ar C), 105.7, 98.4 (Ar CH), 68.2 (CH_2OAr), 62.6 (CH_2OH), 55.5 (OCH_3), 32.5, 28.8, 25.4, 25.4 (CH_2's). IR (CH_2Cl_2): $\nu_{C=O}$ 1677 cm^{-1}. Anal. Calcd for $C_{14}H_{20}O_4$: C, 66.65; H, 7.99. Found: C, 66.69; H, 8.01.

Preparation of 2. A DMF solution (20 mL) of 4-hydroxy-2-methoxybenzaldehyde (1.03 g, 6.8 mmol) was treated with 6-iodohexanol (1.54 g, 6.8 mmol) and K_2CO_3 (3.00 g, 20.2 mmol). The reaction mixture was allowed to react at 50 °C with stirring for 12 h. The mixture was diluted with water (100 mL) and extracted with ether (2 × 150 mL). The organic layers were combined, washed with brine, and dried over anhydrous $MgSO_4$. The solvents were removed under reduced pressure, and the crude product was recrystallized from EtOAc/hexanes (1/5, v/v) to afford a white microcrystalline solid (1.71 g, 89%, mp 85–86 °C). ^{1}H NMR ($CDCl_3$): δ 10.28 (s, 1 H, CHO), 7.80 (d, J = 9.2 Hz, 1 H, Ar), 6.53 (dd, J = 2.0 Hz, J = 8.6 Hz, 1 H, Ar), 6.43 (d, J = 2.0 Hz, 1 H, Ar), 4.04 (t, J = 6.3 Hz, 2 H, CH_2OAr), 3.90 (s, 3 H, CH_3), 3.68–3.67 (m, 2 Hz, CH_2OH), 1.86–1.47 (m, 8 H, CH_2's). ^{13}C NMR ($CDCl_3$): δ 188.3 (CHO), 165.7, 163.6 (Ar C), 130.7 (Ar CH), 118.8 (Ar C), 106.1, 98.3 (Ar CH), 68.2 (CH_2OAr), 62.7 (CH_2OH), 55.5 (OCH_3), 32.6, 29.0, 25.8, 25.5 (CH_2's). IR (CH_2Cl_2): $\nu_{C=O}$ 1677 cm^{-1}. Anal. Calcd for $C_{14}H_{20}O_4$: C, 66.65; H, 7.99. Found: C, 66.62; H, 8.03.

Preparation of 3. A CH_2Cl_2 (30 mL) solution of **1** (2.00 g, 7.9 mmol) was treated with $NCCH_2COOH$ (0.68 g, 7.9 mmol) and DCC (1.97 g, 9.5 mmol). The mixture was allowed to react at ambient temperature with stirring for 4 h. Ether (30 mL) was added, and the reaction mixture was filtered through Celite. The solvents were removed under reduced pressure, and the crude product was oiled out from EtOAc/hexanes (1/5, v/v) to afford **2** as a bright yellow viscous oil (2.5 g, 98%). ^{1}H NMR ($CDCl_3$): δ 10.33 (s, 1 H, CHO), 7.82 (d, J = 8.7 Hz, 1 H, Ar), 6.54 (dd, J = 2.2 Hz, J = 8.7 Hz, 1 H, Ar), 6.44 (d, J = 2.2 Hz, 1 H, Ar), 4.24 (t, J = 6.6 Hz, 2 H, CH_2OAr), 4.07 (t, J = 6.3 Hz, 2 H, CH_2CO_2), 3.88 (s, 3 H, CH_3), 3.49 (s, 2 H, CH_2CN), 1.90–1.48 (m, 8 H, CH_2's). ^{13}C NMR ($CDCl_3$): δ 188.3 (CHO), 166.2 (CO_2), 163.2, 163.0, (Ar C), 130.3 (Ar CH), 119.0 (Ar C), 113.0 (CN), 105.9, 98.5 (Ar CH), 68.2 (CH_2O), 66.8 (CH_2-CN), 55.6 (OCH_3), 28.8, 28.2, 25.7, 25.4, 24.7 (CH_2's). IR (CH_2Cl_2): ester $\nu_{C=O}$ 1751 cm^{-1} and aldehyde $\nu_{C=O}$ 1677 cm^{-1}. UV–vis (CH_2Cl_2): λ_{max} = 314 nm (ϵ = 5.5 × 10^3). Anal. Calcd for $C_{17}H_{21}O_5$: C, 63.94; H, 6.63. Found: C, 64.45; H, 6.78.

Preparation of 4. A CH_2Cl_2 (15 mL) solution of **2** (1.14 g, 4.5 mmol) was treated with $NCCH_2COOH$ (0.38 g, 4.5 mmol) and DCC (1.12 g, 5.4 mmol). The reaction mixture was allowed to react at ambient temperature with stirring for 4 h. Ether (20 mL) was added, and the reaction mixture was filtered through Celite. The solvents were removed under reduced pressure, and the crude solid was recrystallized from EtOAc/hexanes (1/5, v/v) to afford **4** as a bright yellow crystalline solid (1.43 g, 99%, mp 94–95 °C). ^{1}H NMR ($CDCl_3$): δ 10.25 (s, 1 H, CHO), 7.75 (d, J = 8.6 Hz, Ar), 6.50 (dd, J = 1.7 Hz, J = 8.9 Hz, 1 H, Ar), 6.42 (d, J = 2.0 Hz, 1 H, Ar), 4.20 (t, J = 6.6 Hz, 2 H, CH_2OAr), 4.00 (t, J = 6.6 Hz, 2 H, CH_2O_2C), 3.87 (s, 3 H, CH_3), 3.44 (s, 2 H, CH_2CN), 1.8–1.43 (m, 8 H, CH_2's). ^{13}C NMR ($CDCl_3$): δ 188.3 (CHO), 165.6 (CO_2), 163.6, 162.9 (Ar C), 130.6 (Ar CH), 118.8 (Ar C), 113.0 (CN), 106.1, 98.2 (Ar CH), 68.0 (CH_2O), 66.8 (CH_2CN), 55.5 (OCH_3), 33.9, 28.8, 28.2, 25.5, 25.4, 24.9 (CH_2's). IR (CH_2Cl_2): ester $\nu_{C=O}$ 1751 cm^{-1} and aldehyde $\nu_{C=O}$ 1677 cm^{-1}. Anal. Calcd for $C_{17}H_{21}O_5$: C, 63.94; H, 6.63. Found: C, 64.02; H, 6.66.

Preparation of 5. A THF (10 mL) solution of **3** (1.00 g, 3.1 mmol) was treated with DMAP (0.38 g, 3.1 mmol) and allowed to react at ambient temperature with constant stirring for 4 h. The reaction mixture was then treated with 5% HCl (20 mL) and extracted with ether (50 mL). The solvents were removed under reduced pressure, and the polymer was precipitated from $CHCl_3$/hexanes (1/5, v/v) at −25 °C to afford **5** as a light yellow crystalline solid (0.94 g, 82%). ^{1}H NMR

($CDCl_3$): δ 8.73 (s, 1 H, =CH), 8.35 (d, J = 9.2 Hz, 1 H, Ar), 6.57 (dd, J = 2.3 Hz, 8.9 Hz, 1 H, Ar), 6.41 (d, J = 2.6 Hz, 1 H, Ar), 4.32 (t, J = 6.9 Hz, 2 H, CH_2OAr), 4.05 (t, J = 5.6 Hz, 2 H, CH_2O_2C), 3.88 (s, 3 H, CH_3), 1.91–0.88 (m, 8 H, CH_2's). ^{13}C NMR ($CDCl_3$): δ 165.6 (CO_2), 163.5, 160.9 (Ar C), 148.6 (=CH), 130.8 (Ar CH), 116.8 (Ar C), 114.0 (CN), 106.2, 98.5 (Ar CH), 97.7 (=C(CN)), 68.5 (CH_2OAr), 65.8 (CH_2O_2C), 55.6 (OCH_3), 31.5, 28.6, 28.2, 25.9, 22.5, 14.0 (CH_2's). IR (CH_2Cl_2): $\nu_{C=O}$ 1719 cm^{-1}. UV–vis (CH_2CH_2): λ_{max} = 370 nm (ϵ = 14.5 × 10^3). Anal. Calcd: N, 4.65. Found: N, 4.82.

Preparation of 6. A THF (10 mL) solution of **4** (0.95 g, 3.0 mmol) was treated with DMAP (0.36 g, 3.0 mmol) and allowed to react at 50 °C with constant stirring for 4 h. The reaction mixture was then treated with 5% HCl (20 mL) and extracted with ether (50 mL). The solvents were removed under reduced pressure, and the polymer was precipitated from $CHCl_3$/hexanes (1/5, v/v) at −25 °C to afford a yellow microcrystalline solid (0.77 g, 86%). ^1H NMR ($CDCl_3$): δ 8.66 (s, 1 H, =CH), 8.35 (d, J = 8.6 Hz, 1 H, Ar), 6.57 (dd, J = 2.3 Hz, J = 8.9 Hz, 1 H, Ar), 6.44 (d, J = 2.0 Hz, 1 H, Ar), 4.30 (t, J = 6.6 Hz, 2 H, CH_2OAr), 4.06 (t, J = 6.3 Hz, 2 H, CH_2O_2C), 3.88 (s, 3 H, CH_3), 1.84–0.88 (m, 8 H, CH_2's). ^{13}C NMR ($CDCl_3$): δ 165.4 (CO_2), 163.7, 161.4 (Ar C), 148.7 (=CH), 131.0 (Ar CH), 116.8 (Ar C), 113.7 (CN), 106.5, 98.4 (Ar CH), 97.5 (=C(CN)), 68.2 (CH_2OAr), 65.8 (CH_2O_2C), 55.7 (OCH_3). IR (CH_2Cl_2): $\nu_{C=O}$ 1719 cm^{-1}. UV–vis (CH_2Cl_2): λ_{max} = 370 (ϵ = 18.8 × 10^3). Anal. Calcd: N, 4.65. Found: N, 4.65.

Acknowledgment. Support of this research by the Office of Naval Rsearch and the National Science Foundation (PFF program) is gratefully acknowledged by H.S.L. M.E.W. wishes to acknowledge support from the Office of Naval Research and the donors to the Petroleum Research Fund, administered by the American Chemical Society.

References and Notes

(1) For a general treatment of NLO materials see: *NLO Optical and Electroactive Polymers*; Prasad, P. N., Ulrich, D. R.; Eds.; Plenum Press: New York, 1988. *Organic Materials for Nonlinear Optics*, Hann, R. A., Bloor, D., Eds.; Special Publication No. 69), The Royal Society of Chemistry: London, 1989. *Organic Materials* for *Non-linear Optics II*; Hann, R. A., Bloor, D., Eds.; Special Publication No. 91), The Royal Society of Chemistry: London, 1991. *Materials for Non-linear Optics: Chemical Perspectives*; Marder, S. R., Sohn, J. E., Stucky, G. D., Eds.; ACS Symposium, Series 445; American Chemistry Society: Washington, DC, 1991 (see also references cited therein). Also see examples in: *Polym. Prepr. (Am. Chem. Soc., Div. Polym. Chem.)* **1991**, *32* (2), 61–62. Williams, D. J. *Thin Solid Films* **1992**, *216*, 117.

(2) Lytel, R.; Lipscomb, G. F.; Kenny, J. T.; Ticknor, A. *J. Proc. SPIE.* **1991**, *1563*, 122 and references cited therein. Stamatoff, J.; DeMartino, R.; Hass, D.; Khanarian, G.; Man, H. T.; Norwood, R.; Yoon, H. N. *Die Angew. Makromol. Chem.* **1990**, *183*, 151 and references cited therein.

(3) (a) Fuso, F.; Padias, A. B.; Hall, H. K., Jr. *Macromolecules* **1991**, *24*, 1710. (b) Ni, Z.; Leslie, T. M.; Padias, A. B.; Hall, H. K., Jr. *Macromolecules* **1991**, *24*, 2100. (c) Green, G. D.; Hall, H. K., Jr.; Mulvaney, J. E.; Noonan, J.; Williams, D. J. *Macromolecules* **1987**, *20*, 716. (d) Green, G. D.; Weinschenk, J. I.; Mulvaney, J. E.; Hall, H. K., Jr. *Macromolecules* **1987**, *20*, 722. (e) Hall, H. K., Jr.; Padias, A. B.; Fuso, F.; Ni, Z.; Mitchell, M. A.; Leslie, T. M. In *Multifunctional Materials*; Buckley, A., Gallagher-Daggit, G., Karasz, F. E., Ulrich, D. R., Eds. Materials Research Society Symposia Proceedings; Elsevier: New York, 1990; Vol. 175, p 51.

(4) (a) Stenger-Smith, J. D.; Fischer, J. W.; Henry, R. A.; Hoover, J. M.; Lindsay, G. A.; Hayden, L. M. *Makromol. Chem. Rapid Commun.* **1990**, *11*, 141. (b) Lindsay, G. A.; Fischer, J. W.; Henry, R. A.; Hoover, J. M.; Kubin, R. F.; Seltzer, M. D.; Stenger-Smith, J. D. *Polym. Prepr. (Am. Chem. Soc., Div. Polym. Chem.)* **1991**, *32* (2), 91. Lindsay, G. A.; Stenger-Smith, J. D.; Henry, R. A.; Hoover, J. M.; Kubin, R. F. *SPIE-Int. Soc. Opt. Eng. Proc.* **1991**, *1497*, 418–422. Lindsay, G. A.; Nee, S. F.; Hoover, J. M.; Stenger-Smith, J. D.; Henry, R. A.; Kubin, R. F.; Seltzer, M. D. *Ibid.* **1991**, *1560*, 443.

(5) Loucif-Saibi, R.; Nakatani, R. K.; Delaire, J. A.; Dumont, M.; Sekkat, Z. *Chem. Mater.* **1993**, *5*, 229.

(6) Kohler, W.; Robello, D. R.; Dao, P. T.; Willand, C. S.; Williams, D. J. *J. Chem. Phys.* **1990**, *93*, 9157.

(7) Wright. M. E.; Mullick, S.; Lackritz, H. S.; Liu, L-Y. *Macromolecules* **1994**, *27*, 3009. For some recent examples of side-chain NLO polymer see: Hayden, L. M.; Sauter, G. F.; Ore, F. R.; Pasillas, P. L.; Hoover, J. M.; Lindsay, G. A.; Henry, R. A. *J. Appl. Phys.* **1990**, *68*, 456. Zhende, N.; Leslie, T. M.; Padias, A. B.; Hall, H. K., Jr. *Macromolecules* **1991**, *24*, 2100. Zhoa, M.; Bautista, M.; Ford, W. T. *Macromolecules* **1991**, *24*, 844. Allcock, H. R.; Dembek, A. A.; Kim, C.; Devine, R. L. S.; Shi, Y.; Steier, W. H.; Spangler, C. W. *Macromolecules* **1991**, *24*, 1000. Wright, M. E.; Toplikar, E. G.; Kubin, R. F.; Seltzer, M. D. *Macromolecules* **1992**, *25*, 1838.

(8) Wright, M. E.; Toplikar, E. G. *Materials for Nonlinear Optics: Chemical Perspectives*; Marder, S. R., Sohn, J. E., Stucky, G. D., Eds.; ACS Symposium Series 455; American Chemical Society: Washington, DC, 1991; p 602. Wright, M. E.; Toplikar, E. G. *Macromolecules* **1992**, *25*, 6050. Wright, M. E.; Sigman, M. S.; *Macromolecules* **1992**, *25*, 6055. Wright, M. E.; Mullick, S. *Macromolecules* **1992**, *25*, 6045.

(9) Kohler, W.; Robello, D. R.; Dao, P. T.; Willand, C. S.; Williams, D. J. *Macromolecules* **1991**, *24*, 4589.

(10) Katz, H. E.; Schilling, M. L.; Fang, T.; Holland, W. R.; King, L.; Gordon, H. *Macromolecules* **1991**, *24*, 1201. Katz, H. E.; Lavell, W. T. *J. Org. Chem.* **1989**, *56*, 2282. Schilling, M. L.; Katz, H. E. *Materials* **1989**, *1*, 668. Katz, H. E.; Schilling, M. L. *J. Am. Chem. Soc.* **1989**, *111*, 7554.

(11) Xu, C.; Wu, B.; Dalton, L. R.; Shi, Y.; Ranon,; P. M.; Steier, W. H. *Macromolecules* **1991**, *24*, 5421. Xu, C.; Wu, B.; Dalton, L. R.; Ranon, P. M.; Shi, Y.; Steier, W. H. *Macromolecules* **1992**, *25*, 6716.

(12) Francis, C. V.; White, K. M.; Newmark, R. A.; Stephens, M. G. *Macromolecules* **1993**, *26*, 4379.

(13) Hampsch, H. L.; Yang, J.; Wong, G. K.; Torkelson, J. M. *Macromolecules* **1988**, *21*, 526. Hampsch, H. L.; Yang, J.; Wong, G. K.; Torkelson, J. M. *Polym. Commun.* **1989**, *30*, 40. Hampsch, H. L.; Torkelson, J. M.; Bethke, S. J.; Grubb, S. G. *J. Appl. Phys.* **1990**, *67*, 1037. Hampsch, H. L.; Yang, J.; Wong, G. K.; Torkelson, J. M. *Macromolecules* **1990**, *23*, 3640. Hampsch, H. L.; Yang, J.; Wong, G. K.; Torkelson, J. M. *Macromolecules* **1990**, *23*, 3648. Lackritz, H. S.; Torkelson, J. M. In Polymer Physics of Poled Polymers for Second Order Nonlinear Optics. *Molecular Optoelectronics: Materials Physics, and Devices*, Zyss, J., Ed.; Academic Press: New York, 1993; Chapter 8. Loucif-Saibi, R.; Nakatani, K.; Delaire, J. A.; Dumont, M.; Sekkat. Z. *Chem. Mater.* **1993**, *5*, 229.

(14) (a) Prasad, P. N.; Williams, D. J. *Introduction to Nonlinear Optical Effects in Molecules and Polymers*; John Wiley & Sons: New York, 1991. (b) Williams, D. J. *Angew. Chem., Int. Ed. Engl.* **1984**, *23*, 690.

(15) *Reagents for Organic Synthesis*; Fieser, L. F., Fieser, M., Eds.; Wiley: New York, 1967; Vol. 1, p 216. Zentel, R.; Baumann, H.; Scharf, D.; Eich, M.; Schonfeld, A.; Kremer, F. *Makromol. Chem., Rapid Commun.* **1993**, *14*, 121–131.

(16) Giacometti, J. A.; Oliveira, O. N., Jr. *IEEE Trans. Electr. Insul.* **1992**, *27*, 924.

(17) Liu, L.-Y.; Ramkrishna, D.; Lackritz, H. S. *Macromolecules* **1994**, *27*, 5987.

(18) (a) Reiser, A.; Lock, M. W. B.; Knight, J. *Trans Faraday Soc.* **1969**, *65*, 2168. (b) von Seggern, H. *J. Appl. Phys.* **1979**, *50*, 2817. (c) von Seggern, H. *J. Appl. Phys.* **1981**, *52*, 4081. (d) Weiss, D. S. *J. Imaging Sci.* **1990**, *34*, 132. (e) Das-Gupta, D. K. *IEEE Trans. Electr. Insul.* **1992**, *27*, 909. (f) Kasap, S. O. *J. Phys. D: Appl. Phys.* **1992**, *25*, 83.

(19) (a) Kohlrausch, F. *Prog. Ann. Phys.* **1847**, *12*, 393. (b) Williams, G.; Watts, D. C. *Trans. Faraday Soc.* **1970**, *66*, 80. (c) Williams, G.; Watts, D. C. In *NMR Basic Principles and Progress*; Diehl, P., et al., Eds.; Springer-Verlag: New York, 1970; Vol. 4. (d) Matsuoka, S.; Williams, G.; Johnson, G. E.; Anderson, E. W.; Furukawa, T. *Macromolecules* **1985**, *18*, 2652.

(20) (a) Dhinojwala, A.; Wong, G. K.; Torkelson, J. M. *Macromolecules* **1993**, *26*, 5943. (b) Dhinojwala, A.; Wong, G. K.; Torkelson, J. M. *J. Chem. Phys.* **1994**, *100*, 6046.

(21) McCrum, N. G.; Read, B. E.; Williams, G. *Anelastic and Dielectric Effects in Polymeric Solids*; Dover Publications: New York, 1991.

(22) Jonscher, A. K. *Philos. Mag. B* **1978**, *38*, 587.

MA945030Z